Solar-Terrestrial Physics. 2019. Vol. 5. Iss. 1. P. 58–61. DOI: 10.12737/stp-51201908. © 2019 Zh.V. Dashkevich, V.E. Ivanov. Published by INFRA-M Academic Publishing House
Original Russian version: Zh.V. Dashkevich, V.E. Ivanov, published in Solnechno-zemnaya fizika. 2019. Vol. 5. Iss. 1. P. 77–81. DOI: 10.12737/szf-51201908. © 2019 INFRA-M Academic Publishing House (Nauchno-Izdatelskii Tsentr INFRA-M)

ESTIMATED NITRIC OXIDE DENSITY IN AURORAS FROM GROUND-BASED PHOTOMETRIC DATA

Zh.V. Dashkevich
Polar Geophysical Institute RAS, Apatity, Russia, zhanna@pgia.ru

V.E. Ivanov
Polar Geophysical Institute RAS, Apatity, Russia, ivanov@pgia.ru

Abstract. In this paper, we numerically estimate the nitric oxide density in auroras, using photometric data on 427.8, 557.7, and 630.0 nm emission intensities. The data were obtained at midnight at observatories of the Polar Geophysical Institute. These estimates were made using a numerical modeling procedure with a time-dependent model of the auroral ionosphere [Dashkevich et al., 2017]. It is shown that the NO density in the maximum of the altitude profile is between $(1\div3.3)\cdot10^8$ cm^{-3}. The obtained estimates indicate the absence of a correlation between the $[NO]_{max}$ values and 427.8 nm emission intensities.

Keywords: nitric oxide, ionospheric component densities, auroras, emission intensity, modeling, electron precipitation.

INTRODUCTION

The nitric oxide (NO) as a small component of the atmosphere plays an important role in the cycle of physico-chemical processes occurring during auroral electron precipitation in the ionosphere. There are no direct mass spectrometric measurements of NO density in auroras. The NO content in the auroral region was estimated by analyzing rocket measurements of ionic composition in the atmosphere or NO_2 continuum intensity in the 520.0 nm emission [Sharp, 1978; Swider, Narcisi, 1977], as well as satellite measurements of NO intensity [Gerard, Barth, 1977; Gerard, Noel, 1986; Rusch, Barth, 1975; Siskind et al., 1989; Solomon et al., 1999; Stevens et al., 1997]. Figure 1 shows the [NO] altitude profiles obtained from measurements made directly in auroras. We can see that [NO] in the profile maximum can vary in the range of 10^7–10^9 cm^{-3}.

Dashkevich and Ivanov [2017] have described in detail a method capable of estimating [NO] in auroras from measurements of 1NG $N_2^+\left(B^2\Sigma_u^+\right)$391.4 nm, OI (^{1}S) 557.7, and OI (^{1}D) 630.0 nm emission intensities. This method relies on the fact that NO is an ion absorber O_2^+: $O_2^+ + NO \rightarrow NO^+ + O_2$, whose dissociative recombination $O_2^+ + e \rightarrow O\left(^1S\right) + O\left(^1D\right)$ is one of the major sources of atomic oxygen in the ^{1}S state, which, in turn, is a source of the 557.7 nm emission. In this paper, we present the [NO] estimates obtained from auroral measurements of 1NG $N_2^+\left(B^2\Sigma_u^+\right)$ 427.8 nm, OI (^{1}S) 557.7 nm, and OI (^{1}D) 630.0 nm emission intensities. The estimates were made by modeling the redistribution of internal freedom degrees of the excited atmospheric gas energy released in the ionosphere due to auroral electron precipitation. Using the measured 427.8, 557.7, and 630.0 nm emission intensities, we reconstructed the energy spectra of precipitated electrons and [NO], which represented the auroral emission intensities.

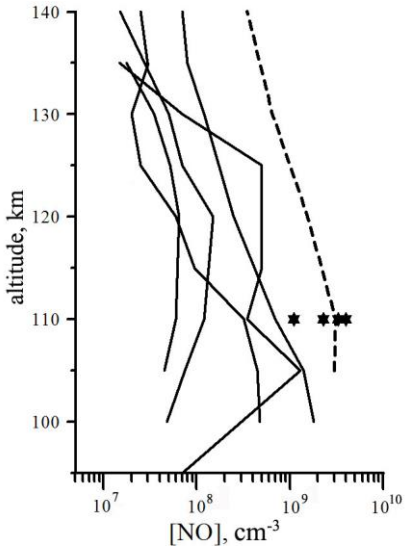

Figure 1. NO density as a function of height: asterisks indicate data from [Sharp, 1978] obtained from $\left[NO^+\right]/\left[O_2^+\right]$, the dashed line shows data on the NO_2 continuum emission intensity from [Sharp, 1978]; solid lines, data from [Swider, Narcisi, 1977]

MODELING RESULTS

To estimate [NO], we have used photometric observations of 427.8, 557.7, and 630.0 nm emission intensities in auroras. The observations were made at observatories of the Polar Geophysical Institute in 1998–2001. Data on emission intensity at zenith were acquired at midnight, with aurora glowing and in the absence of cloudiness. The experimental data set contains 1335 measurements in eight nighttime series of observations at Lovozero Observatory (Φ'=64.17° N) and 1200 measurements in eight nighttime series at the Tumanny Observatory (Φ'=65.24° N). Details of the experimental data processing are given in [Dashkevich et al., 2006]. Here we note only that the 427.8 nm emission intensity is in the range 0.1–2 kR. The measurements averaged

over the two stations and grouped in 427.8 nm emission intensities are presented in the first three columns of Table 1. The range of the 427.8 nm emission intensity variation is divided into intervals of 100 R.

[NO] and 427.8, 557.7, and 630.0 nm emission intensities in the electron precipitation region were calculated using a numerical modeling procedure with the physico-chemical model describing the interaction between the main excited and ionized atmospheric components during electron precipitation [Dashkevich et al., 2017]. The model is based on the data available in the scientific literature and contains 56 physico-chemical reactions, including 23 reactions involving the odd nitrogen NO, $N(^4S)$, $N(^2D)$, $N(^2P)$, N^+, and NO^+. The reactions included in this model and describing the redistribution of the auroral electron energy released in the ionosphere are listed in Table 2. A distinctive feature of this model is a method for calculating vertical profiles of atmospheric gas excitation rates, which is based on the functional allowing us to analytically relate the altitude profiles of excited atmospheric components to the energy spectrum of precipitating electrons [Sergienko, Ivanov, 1993]. The numerical model calculates the altitude profiles of density of ionospheric components N_2^+, O_2^+, $O^+(^4S)$, $O^+(^2D)$, $O^+(^2P)$, $O(^1D)$, $O(^1S)$, $N(^4S)$, $N(^2D)$, $N(^2P)$, NO, NO^+, N^+, $N_2(A^3\Sigma_u^+)$, $N_2(B^3\Pi_g)$, $N_2(W^3\Delta_u)$, $N_2(B'^3\Sigma_u^-)$, $N_2(C^3\Pi_u)$ and electrons in the auroral ionosphere; the temporal dynamics of density of ionospheric components; altitude profiles of intensity of the main auroral emissions, including 427.8, 557.7, and 630.0 nm. Since the model ignores transfer effects, it can be applied to E and lower F layers of the ionosphere. Input parameters of the model are a model of the neutral atmosphere and parameters of precipitating electron flux.

In this work, we use the model of the neutral atmosphere MSIS-90 and the energy spectrum of precipitating electrons in the form of Maxwellian distribution

$$N(E) = N_0 E \exp(-E/E_0)/E_0^2, \quad (1)$$

where N_0 and E_0 are the precipitating electron flux at the upper boundary of the thermosphere ($cm^{-2}s^{-1}$) and the characteristic energy (eV) respectively.

The procedure for reconstructing the [NO] vertical profiles, described in detail in [Dashkevich, Ivanov, 2017], consists of two stages. At the first stage, we determine parameters of precipitating electron flux (1), specified in the model, namely the characteristic energy E_0 and the particle flux N_0, which provide the 427.8 and 630.0 nm emission intensities observed in the experiment. The characteristic energy E_0 is estimated from the experimentally obtained intensity ratios $I_{630.0}/I_{427.8}$. As can be seen from [Dashkevich et al., 2006; Dashkevich, Ivanov, 2017; Eather, Mende, 1972; Rees, Luckey, 1974], $I_{630.0}/I_{427.8}$ is virtually independent of N_0 and is determined by E_0. Moreover, Dashkevich and Ivanov [2017] have shown that $I_{630.0}/I_{427.8}$ is also independent of [NO]. Figure 2 shows the E_0 dependence of $I_{630.0}/I_{427.8}$ we use, which was calculated according to the physico-chemical model of the ionosphere [Dashkevich et al., 2017]. Values of N_0 fluxes are found from the condition

$$I_{427.8}^{exp} = N_0 \iint \eta_{427.8}^{theor}(E, h) E \exp(-E/E_0)/E_0^2 dE dh,$$

where $I_{427.8}^{exp}$ is the experimentally measured 427.8 nm emission intensity ($cm^{-2}s^{-1}$); $\eta_{427.8}^{theor}(E, h)dEdh$ is the volume emission at 427.8 nm, produced by precipitating electrons with energies from E to $E+dE$ at a height h in a layer dh thick; E_0 is the characteristic energy (eV).

Table 1

Modeling results

$I_{427.8}$, Рл exp.	$I_{557.7}$, R exp.	$I_{630.0}$, Рл exp.	E_0, eV calc.	N_0, 10^9 $cm^{-2}s^{-1}$ calc.	$[NO]_{max}$, 10^8 cm^{-3} calc.	$I_{557.7}$, R calc.
150	782	273	1039	0.5	1.6	780
250	1330	365	1116	0.8	1.6	1330
350	1845	403	1291	0.9	1.8	1845
450	2437	475	1370	1.1	1.7	2432
550	2945	490	1541	1.2	2.3	2941
650	3551	544	1607	1.3	2.2	3543
750	4075	650	1559	1.5	2.2	4072
850	4930	609	1780	1.5	1.5	4927
950	5567	578	1987	1.5	1.4	5554
1100	6683	737	1858	1.9	1.0	6679
1350	7755	744	2102	2.0	1.7	7754
1700	9243	745	2465	2.1	3.3	9223

Table 2

Reactions of interaction of atmospheric ions with excited components in auroras

N_2^+	$O^+(^2P)$	$N(^4S)$
$N_2^+ + O_2 \rightarrow N_2 + O_2^+$	$O^+(^2P) + N_2 \rightarrow O^+(^4S) + N_2$	$N(^4S) + O_2 \rightarrow NO + O$
$N_2^+ + O \rightarrow N_2 + O^+(^4S)$	$O^+(^2P) + N_2 \rightarrow N_2^+ + O$	$N(^4S) + NO \rightarrow N_2 + O$
$N_2^+ + O \rightarrow NO^+ + N(^2D)$	$O^+(^2P) + O \rightarrow O^+(^4S) + O$	$N(^2D)$
$N_2^+ + NO \rightarrow N_2 + NO^+$	$O^+(^2P) + O_2 \rightarrow O_2^+ + O$	$N(^2D) + O_2 \rightarrow NO + O(^3P, ^1D)$
$N_2^+ + e \rightarrow N(^4S) + N(^2D)$	$O^+(^2P) \rightarrow O^+(^2D) + h\nu$	$N(^2D) + O \rightarrow N(^4S) + O(^3P, ^1D)$
O_2^+	$O^+(^2P) \rightarrow O^+(^4S) + h\nu$	$N(^2D) + NO \rightarrow N_2 + O$
$O_2^+ + e \rightarrow O(^1S) + O(^1D)$	$O^+(^2P) + e \rightarrow O^+(^2D) + e$	$N(^2D) + NO \rightarrow N(^4S) + NO$
$O_2^+ + N(^4S) \rightarrow NO^+ + O(^1S)$	$O^+(^2P) + e \rightarrow O^+(^4S) + e$	$N(^2D) + e \rightarrow N(^4S) + e$
$O_2^+ + NO \rightarrow NO^+ + O_2$	$O(^1D)$	$N(^2D) \rightarrow N(^4S) + h\nu$
$O_2^+ + N(^2D) \rightarrow NO^+ + O$	$O(^1D) + N_2 \rightarrow O + N_2$	$N(^2P)$
$O^+(^4S)$	$O(^1D) + O_2 \rightarrow O + O_2$	$N(^2P) + O_2 \rightarrow NO + O(^1S, ^1D, ^3P)$
$O^+(^4S) + N_2 \rightarrow NO^+ + N(^4S)$	$O(^1D) + O \rightarrow O + O$	$N(^2P) + O \rightarrow N(^2D) + O$
$O^+(^4S) + O_2 \rightarrow O_2^+ + O$	$O(^1D) \rightarrow O + h\nu$	$N(^2P) \rightarrow N(^2D) + h\nu$
$O^+(^4S) + NO \rightarrow NO^+ + O$	$O(^1D) + e \rightarrow O + e$	$N(^2P) \rightarrow N(^4S) + h\nu$
$O^+(^2D)$	$O(^1S)$	$N(^2P) + NO \rightarrow N_2 + O$
$O^+(^2D) + N_2 \rightarrow N_2^+ + O$	$O(^1S) + O \rightarrow O + O$	N^+
$O^+(^2D) + N_2 \rightarrow NO^+ + N(^4S)$	$O(^1S) \rightarrow O(^1D) + h\nu$	$N^+ + O_2 \rightarrow O_2^+ + N(^4S, ^2D)$
$O^+(^2D) + O_2 \rightarrow O_2^+ + O$	$O(^1S) \rightarrow O + h\nu$	$N^+ + O_2 \rightarrow NO^+ + O(^1D, ^1S)$
$O^+(^2D) + O_2 \rightarrow O^+(^4S) + O_2$	$O(^1S) + O_2 \rightarrow O + O_2$	$N^+ + O_2 \rightarrow O^+(^4S) + NO$
$O^+(^2D) + O \rightarrow O^+(^4S) + O$	$O(^1S) + NO \rightarrow O + NO$	$N^+ + O \rightarrow O^+(^4S) + N(^4S)$
$O^+(^2D) + e \rightarrow O^+(^4S) + e$	NO^+	$N_2(A^3\Sigma_u^+)$
$O^+(^2D) \rightarrow O^+(^4S) + h\nu$	$NO^+ + e \rightarrow O + N(^4S, ^2D)$	$N_2(A^3\Sigma_u^+) + O \rightarrow N_2 + O(^1S)$

Note. Reaction rate constants are shown in [Dashkevich et al., 2017].

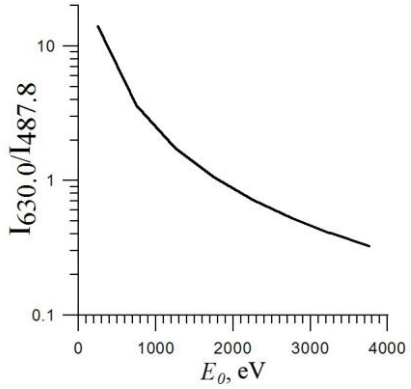

Figure 2. The intensity ratio $I_{630.0}/I_{427.8}$ versus E_0

The E_0 and N_0 values thus determined provide the experimentally observed intensities $I_{427.8}$ and $I_{630.0}$ for precipitating electrons with the given energy spectrum in the form of (1).

The second stage involves calculating altitude profiles of the 557.7 nm emission intensity and respective vertical distributions of [NO]. The absolute values of [NO] for each event are determined by the condition that the best agreement is obtained between the calculated values of $I_{557.7}$ and those measured in the experiment. The [NO] vertical profiles thus modeled are depicted in Figure 3. The calculated values of $[NO]_{max}$ in

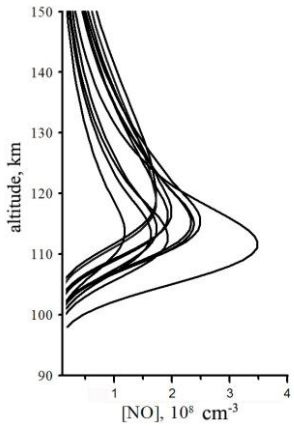

Figure 3. Modeled altitude profiles of [NO]. Each curve corresponds to one pair of ratios $I_{630.0}/I_{427.8}$ and $I_{557.7}/I_{427.8}$

the maximum of the altitude profile are shown in Table 1. For comparison we give the modeled values of $I_{557.7}$. Estimates of [NO] in auroras, obtained from photometric measurements of $I_{427.8}$, $I_{557.7}$, and $I_{630.0}$, are seen to be within $(1\div3.3)10^8$ cm^{-3} for $I_{427.8}$ ranging from 0.1 to 2 kR. The results agree satisfactorily with the [NO] estimates, obtained from the analysis of the ion composition in auroras, measured in rocket experiments [Sharp, 1978; Swider, Narcisi, 1977].

It should also be noted that the results we got indicate that there is no direct correlation between $I_{427.8}$ and $[NO]_{max}$. This fact has been discussed by Gerard and Barth [1977]. The cause of the absence of this correlation can be explained by the long lifetime of NO, which can accumulate in the ionosphere. Therefore, [NO] in each particular aurora may be determined not only by the duration and intensity of precipitated electron fluxes, but also by the duration and intensity of auroral activity preceding the event under study.

CONCLUSIONS

This paper presents numerical estimates of the NO content in auroras, obtained from ground photometric measurements of 427.8, 557.7, and 630.0 nm emission intensities in the midnight sector of the auroral oval. We have shown that [NO] in the maximum of its vertical profile $[NO]_{max}$ is within $(1\div3.3)\cdot10^8$ cm^{-3}. We found no direct correlation between $[NO]_{max}$ and 427.8 nm emission intensities.

REFERENCES

Dashkevich Zh.V., Ivanov V.E. Estimation of the NO concentration in the polar region from 391.4, 557.7, and 630.0 nm emission intensities. *Cosmic Res.* 2017, vol. 55, no. 5, pp. 318–322. DOI: 10.1134/S0010952517050045.

Dashkevich Zh.V., Zverev V.L., Ivanov V.E. Ratios of $I_{630.0}/I_{427.8}$ and $I_{557.7}/I_{427.8}$ emission intensities in auroras. *Geomagnetism and Aeronomy*. 2006, vol. 46, no. 3, pp. 366–370. DOI: 10.1134/S001679320603011X.

Dashkevich Zh.V., Ivanov V.E, Sergienko T.I., Kozelov B.V. Physicochemical model of the auroral ionosphere. *Cosmic Res*. 2017, vol. 55, no. 2, pp. 88–100. DOI: 10.1134/S0010952517020022.

Eather R.H., Mende S.B. Systematics in auroral energy spectra. *J. Geophys. Res*. 1972, vol. 77, no. 4, pp. 660–673. DOI: 10.1029/JA077i004p00660

Gérard J.-C., Barth C.A. High-latitude nitric oxide in the lower thermosphere. *J. Geophys. Res*. 1977, vol. 82, no. 4, pp. 674–680. DOI: 10.1029/JA082i004p00674.

Gérard J.-C., Noel C.E. AE-D measurements of the NO geomagnetic latitudinal distribution and contamination by $N^+(^5S)$ emission. *J. Geophys. Res*. 1986, vol. 91, no. A9, pp. 10136–10140. DOI: 10.1029/JA091iA09p10136.

Rees M.H., Luckey D. Auroral electron energy derived from ratio of spectroscopic emissions. 1. Model computations. *J. Geophys. Res*. 1974, vol. 79, no. 34, pp. 5181–5186. DOI: 10.1029/JA079i034p05181.

Rusch D.W., Barth C.A. Satellite measurements of nitric oxide in the polar region. *J. Geophys. Res*. 1975, vol. 80, no. 25, pp. 3719–3721. DOI: 10.1029/JA080i025p03719.

Sergienko T.I., Ivanov V.E. A new approach to calculate the excitation of atmospheric gases by auroral electron impact. *Ann. Geophys*. 1993, vol. 11, no. 8, pp. 717–727.

Sharp W.E. NO_2 continuum in aurora. *J. Geophys. Res.* 1978, vol. 83, no. 9, pp. 4373–4376. DOI: 10.1029/JA083iA09p04373.

Siskind D.E., Barth C.A., Evans D.S., Roble R.G. The response of the thermospheric nitric oxide to an auroral storm. 2. Auroral latitudes. *J. Geophys. Res.* 1989, vol. 94, no. A12, pp.16899–16911. DOI: 10.1029/JA094iA12p16899.

Solomon C.S., Barth C.A., Bailey S.M. Auroral production of nitric oxide measured by the SNOE satellite. *Geophys. Res. Lett.* 1999, vol. 26, pp. 1259–1262. DOI: 10.1029/1999GL900235.

Stevens M.H., Conway R.R., Cardon J.G., Russell J.M. MAHRSI observations of nitric oxide in the mesosphere and lower thermosphere. *Geophys. Res. Lett*. 1997, vol. 24, pp. 3213–3216. DOI: 10.1029/97GL03257.

Swider W., Narcisi R.S. Auroral E-region: Ion composition and nitric oxide. *Planet. Space Sci*. 1977, vol. 25, no. 2, pp. 103–116. DOI: 10.1016/0032-0633(77)90014-9.

How to cite this article

Dashkevich Zh.V., Ivanov V.E. Estimated nitric oxide density in auroras from ground-based photometric data. *Solar-Terrestrial Physics*. 2019. Vol. 5. Iss. 1. P. 58–61. DOI: 10.12737/stp-51201908.